Electrochemically synthesized mesoporous thin films of ZnO for highly efficient dye sensitized solar cells

F. Anderson S. Lima[a,b,*], Igor F. Vasconcelos[a], M. Lira-Cantu[b]

[a]Dep. Eng. Metalúrgica e de Materiais, Universidade Federal do Ceará, Campus do Pici Bloco 714, 60455-760 Fortaleza, CE, Brazil
[b]Institut Català de Nanociència i Nanotecnologia, Campus de la UAB, Edifici ICN2 08193 Bellaterra, BCN, Spain

Abstract

In this work, nanostructured thin films of ZnO were electrochemically grown on FTO substrates. The morphology was tuned by modifying the synthesis parameters. The synthesis was carried out by applying $Zn(NO_3) \cdot 6H_2O$ as the sole component of the aqueous electrolyte, avoiding the use of capping agents. The composition and morphology of the prepared ZnO were characterized by energy-dispersive X-ray spectroscopy (EDX) and scanning electron microscopy (SEM), respectively. The as-deposited films were applied as electrodes in dye sensitized solar cells (DSCs). The performance of the cells was investigated by $J \times V$ curves and IPCE (incident photon to charge carrier efficiency) measurements. The SEM analysis demonstrated a direct relationship between ZnO morphology and Zn precursor concentration. It has been shown that the lower the concentration is, the more porous the morphology is. Increasing the amount of dye adsorbed on the ZnO decreased the power conversion efficiency of the final DSCs. The best cell presented the following parameters: open circuit voltage $V_{OC} = 0.59\ V$, short circuit current $J_{SC} = 7.64\ mA/cm^2$, fill factor FF$=50.41\%$, and power conversion efficiency PCE$=2.27\%$.

1. Introduction

ZnO has recently emerged as a promising candidate for its application in excitonic solar cells (XSC). Different ZnO nanostructures like nanowires, nanotubes, nanobelts, nanotetrapods, mesoporous thin films, among others have been successfully obtained by low-cost techniques such as the hydrothermal and the electrochemical synthesis routes [1–6]. TiO$_2$ is still the most commonly used semiconductor oxide in XSC applications. However, interest at ZnO XSC has increased in the same rate as it has been investigated and successfully applied in this technology [7–9]. ZnO presents unique properties that are very similar to those of TiO$_2$. In fact, ZnO presents some advantages in comparison with TiO$_2$ like faster charge transport due to electron mobility and conductivity of several orders of magnitude higher than that

observed for TiO$_2$ [10,11]. Among the various synthesis methods developed to produce ZnO nanostructured thin films, the electrodeposition is a very attractive technique due to its low cost, scalability, and low temperature processing. Direct control of film morphology is possible by manipulating the electrodeposition parameters like applied current, applied potential, electrolyte concentration, temperature, and pH [12–15]. Moreover, electrochemical deposition of ZnO permits the fabrication of novel nanostructured thin films with superior advantages like large surface area and electron mobility, and more efficient charge transport [16–20]. Zhu et al. [21] have proved that a combination of nanorod/nanoparticle composite architecture can improve the performance of TiO$_2$ DSCs. Over the last few years, different ZnO nanostructures have been successfully applied in DSCs [22–25].

In this work, thin films of ZnO were obtained by electrodeposition under different synthesis parameters. These films were morphologically, compositionally, and structurally characterized. The photoanodes were finally applied to assemble DSCs.

---

2. Experimental procedure

2.1. Synthesis of nanostructured ZnO thin films

Nanostructured ZnO thin films were fabricated by an electrochemical deposition process. The film deposition was carried out by applying the $Zn(NO_3) \cdot 6H_2O$ as the sole component of the aqueous electrolyte avoiding the use of any capping agent. A Pt foil and a FTO-coated glass from SOLEMS® with sheet resistance of 50–70 Ω/square were used as a counter electrode and a working electrode, respectively. The potential was applied with respect to an Ag/AgCl (KCl-Sat) reference electrode. Three different concentrations of zinc nitrate on the aqueous solution were used: 12.5 mM, 25 mM and 50 mM. The temperature was always kept at 80 °C, through the use of a hot plate and the applied potential for all procedures was -1.0 V. The reaction time ranged from 0.5 h to 2 h. The crystal structure, morphology and composition of the as-deposited ZnO nanostructured thin films were characterized by X-ray diffraction (XRD), scanning electron microscopy (SEM) and energy-dispersive X-ray spectroscopy (EDX) respectively.

2.2. Solar cell fabrication and characterization

As-deposited ZnO thin films were immersed in a 0.5 mM/L ethanolic solution of N719 dye for 1 h in order to provide dye loading at the ZnO. After dye loading, the working electrodes were used to assemble DSSC. The platinized FTO counter electrode was prepared by electron beam physical vapor deposition (EBPVD), with a Pt thickness of 50 nm. The work and counter electrodes were bonded together with a hot melt sealing foil. The commercial liquid iodide-iodine electrolyte was introduced through a small hole on the Pt counter-electrode by capillary forces applying vacuum. Finally, the DSSC were hermetically sealed with a small piece of glass to close the filling hole. Photoelectrochemical tests were carried out by measuring the $J \times V$ characteristic curves under simulated AM 1.5 solar illumination at 100 mW/cm^{-2} from a sun simulator Steuernagel Solarkonstant® KHS1200. $J \times V$ curves were measured using a Keithley® 2601 multimeter. Incident Photon to Charge Carrier Efficiency (IPCE) measurements were carried out with a QE/IPCE measurement system from Oriel® at 10 nm intervals between 300 and 700 nm. The results were not corrected for intensity losses due to light absorption and reflection by the glass support.

3. Results and discussion

3.1. Structural, morphological and compositional analysis

Special attention was given to the optimization of the reaction time and to the concentration of zinc nitrate in the aqueous electrolyte. Samples 1, 2 and 3 were deposited from a 50 mM zinc nitrate electrolyte for 0.5 h (sample 1) and 2 h in 4 steps of 0.5 h each (samples 2 and 3). Sample 2 was cleaned with deionized water and dried with nitrogen between two consecutive 0.5 h steps left standing in air between cycles. Sample 3 was maintained in the electrolyte solution between cycles. For samples 4 and 5, the total

reaction time was 2 h in one single step with concentration of zinc nitrate in the aqueous electrolyte of 25 mM and 12.5 mM respectively. Table 1 summarizes the deposition conditions for the preparation of each electrode.

Fig. 1 shows XRD diffractograms for Samples 3, 4 and 5. The diffractogram corresponding to sample 3 electrode (electrolyte concentration of 50 mM) reveals the existence of a single crystalline phase with hexagonal wurtzite structure (CPDS card file number 36-1451, zincite phase). The maximum intensity for the ZnO corresponds to the (1011) diffraction peak. Therefore, the observation of a strong and narrow (0002) peak suggests that the nanostructure is highly oriented along the c-axis perpendicular to the plane of the substrate ([0001] direction). The diffractograms of samples 4 and 5 (electrolyte concentrations of 25 mM and 12.5 mM) also show a preferential orientation along the (0002) plane but with increasingly lower relative intensity of the (0002) peak. The diffractograms of samples 4 and 5 agree with the presence of ZnO as described before. Extra peaks at 2θ equal to 26.5°, 36.3° and 56.6° correspond to the FTO substrate.

The influence of deposition reaction time and contact with air on film morphology was studied. Films grown from a 50 nM zinc nitrate electrolyte (samples 1, 2, and 3) were used. Fig. 2(a) shows a SEM micrograph (top view) of a sample 1 where it is possible to observe a very dense array of vertically aligned nanorods. A different microstructure was formed in the region between the nanorods as can be seen more clearly on a micrograph taken with a larger magnification and shown in

Table 1
Samples and deposition conditions.

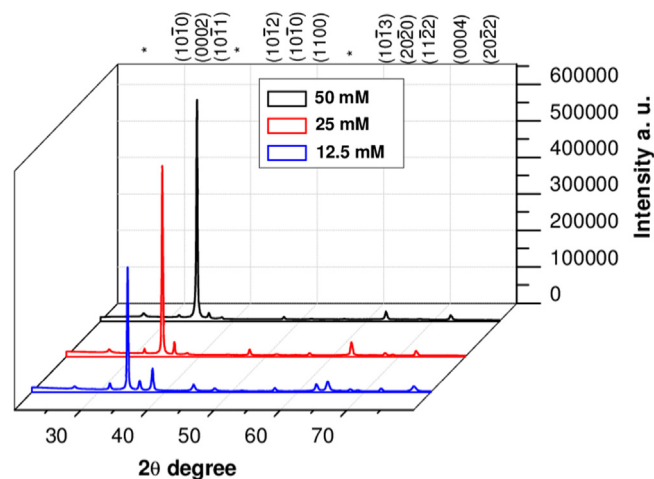| Sample	Electrolyte concentration (mM)	Reaction time (h)	Number of steps	Contact with air
1	50	0.5	1	No
2	50	2	4	Yes
3	50	2	4	No
4	25	2	1	No
5	12.5	2	1	No

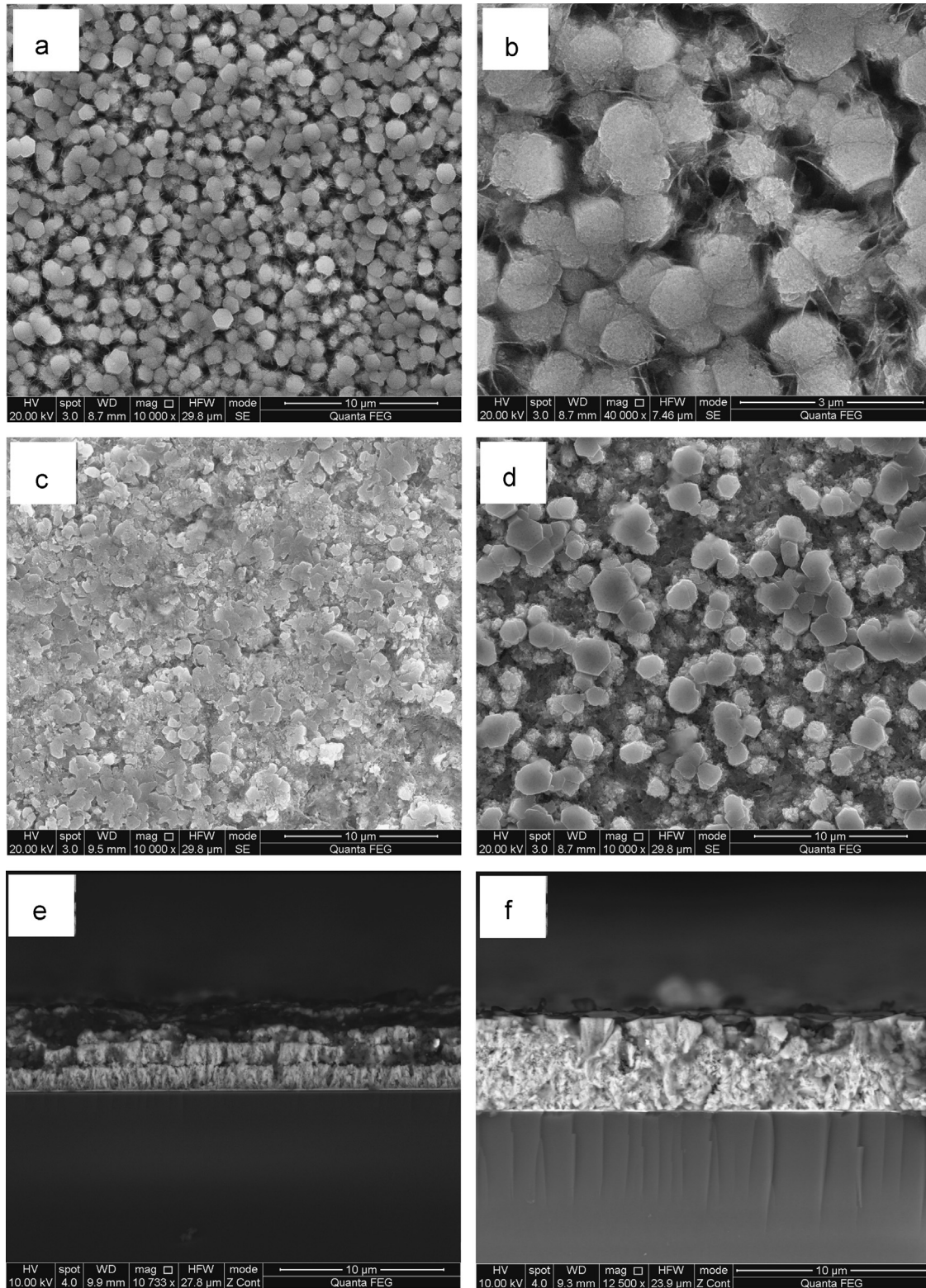Fig. 1. XRD diffractograms for the electrodes from the samples 3, 4 and 5.

Fig. 2. SEM micrographs of electrodes from: (a) sample 1 - top view; (b) sample 1 - top view, higher magnification; (c) sample 2 - top view; (d) sample 3 - top view; (e) sample 2 - cross sectional view; and (f) sample 3 - cross sectional view.

Fig. 2(b). The deposition of vertically aligned nanorods confirms the XRD results and is explained by the fact that ZnO crystallizes with the wurtzite crystal structure, which presents hexagonal symmetry and consists of tetrahedrally coordinated Zn and O atoms in alternating layers along the c-axis. These layers are composed uniquely of either Zn^{2+} or O^{2-} ions and are therefore polar [9]. The polar (0001) plane has higher surface energy and leads to the fast crystal growth

rate along the [0001] direction resulting in the formation of one-dimensional ZnO nanostructures [26].

Although the internal structure of ZnO favors the anisotropic growth along the [0001] direction, the surrounding conditions during the electrodeposition process may affect the growth habit of ZnO [27]. The later could explain the different morphology observed between the nanorods. This growth mechanism can be also responsible for the coalescence between adjacent nanorods observed on the microstructure of the sample 2 as can be clearly seen in the micrograph in Fig. 2(c). Moreover, the growth of a porous nanostructure between the nanorods of sample 3 is observed in Fig. 2(d). According to Ludwig et al. [28] there is a strong correlation between the amount of electrochemically deposited ZnO and the morphology of the thin film. The total amount of electrochemically deposited ZnO can be estimated from the total charge deposited per area (integrated from the monitored current density *versus* time). In this study, the average current density for all the deposited films was 1.3 mA/cm^2. This high current density probably led to a fast growth rate of the ZnO nuclei, and the growth of ZnO along other directions. As a result, the creation of different nanostructures between the nanorods and their coalescence was observed.

Fig. 2(e) shows the cross sectional micrograph for the sample 2. The effect of air contact between consecutive deposition steps is observed by discontinued layers corresponding to each of four 0.5 h steps. As sample 3 was also grown in a four step deposition cycle but maintaining the sample inside the electrolyte (no air contact) between consecutive steps. Thus, the sample does not show discontinued layers as can be seen in the SEM micrograph shown in Fig. 2(f). Air contact influences film composition as well as microstructure as can be seen in Table 2 which shows EDX results on the films deposited with and without air contact (samples 2 and 3, respectively). Films grown with air contact between deposition steps show an excess of oxygen content with respect to zinc while films grown without air contact show stoichiometric ZnO composition. The excess of oxygen can be explained by the reaction of the ZnO surface with oxygen from the air forming an insulating layer of zinc hydroxide (ZnOH) which is an insulator.

The influence of the concentration of zinc precursor on the morphology of the films was also investigated. For this study, films were grown from 25 nM and 12.5 mM electrolytes in a single step of 2 h (samples 4 and 5) with all other parameters kept the same as before. The high density current during the electro-chemical reaction together with the low concentrations of the zinc precursor in the aqueous electrolyte led to novel nanostructures as can be seen in the SEM micrographs shown in Fig. 3. Fig. 3(a) and (b) shows top view images of the electrodes grown from 25 mM and 12.5 mM electrolytes, respectively. In these images, porous films are seen instead of the vertically aligned nanorods found for samples grown from 50 mM electrolytes. The cross

sectional views of these same films that are shown in Fig. 3(c) and (d) do not show vertically aligned structures, which means that the films grown in other directions which not along the *c*-axis. The late is in well agreement with the XRD results that showed a lower relative intensity of the (0002) peaks for these samples. In fact, high resolution SEM images of sample 5 (12.5 mM) presented in Fig. 4 show the formation of a mesoporous nanostructure (see Fig. 4).

3.2. Photovoltaic performance

The electrodes described above were used without any further treatment as photoanodes to construct dye sensitized solar cells (DSCs). The solar cells were tested under simulated AM 1.5 solar illumination at 100 mW/cm^2. Fig. 5 shows $J \times V$ curves and IPCE spectra for the samples using different ZnO layers, while Table 3 shows the photovoltaic parameters for these cells. The data show that all DSCs presented short circuit current density J_{SC} greater than 2.89 mA/cm^2, open circuit potential V_{OC} greater than 0.59 V, fill factor FF greater than 46.58% and power conversion efficiency PCE greater than 0.97%. These values are in good agreement with the ones recently reported for ZnO thin films deposited in a similar way and without any post-deposition treatment [30,31].

The data show that V_{OC} values are approximately the same for all the cells. As the V_{OC} for a DSCs is defined as the difference between the redox potential of the mediator and the Fermi level of the nanocrystalline film [29], it is possible to state that Fermi level energies for all thin films are approximately the same. The data also reveals that J_{SC} values tend to increase with decreasing electrolyte concentration. According to SEM and XRD results, a decrease in electrolyte concentration leads to more porous films which is desired in order to get the best photovoltaic performance. In fact, the solar cell built with sample 4 (12.5 mM), that presented a mesoporous nanostructure, reached the maximum J_{SC} value. Moreover, considering the absence of post-deposition treatment, a remarkably high *PCE* value of 2.27% was obtained for this cell. The improvement on J_{SC} can be attributed to mesoporous structure of the thin film, which allows the absorption of larger amount of dye, as monolayers, on the ZnO nanostructures which provides the generation of more photoelectrons and consequently higher J_{SC}. The series and shunt resistance were determined from the slopes of the I–V curves. The photovoltaic parameters for the DSCs analyzed in this study are presented in Table 3.

The amount of dye adsorbed on the oxide was measured by the dye desorption method, which consists of the separation of the two electrodes, followed by the immersion of the ZnO-dye electrode in an aqueous basic solution of 0.1 mM KOH. The dye desorption took place after 1 h, with the solution turning into a pink color due to the presence of the N719 dye. At the same time, the ZnO electrode turned colorless as was found by Neale et al. [32]. The quantity of dye adsorbed on the ZnO electrode was determined by UV-vis analysis of the desorbed dye solution applying the Lambert–Beer law. The results were corrected by the active area of the DSCs. The relationship between the amount of adsorbed dye and efficiency, for the electrodes grown on the electrolyte containing 50 mM of zinc nitrate, is shown in Fig. 6. The data revealed higher power conversion efficiency for samples with the

Table 2
EDX results for the composition of some ZnO electrodes.

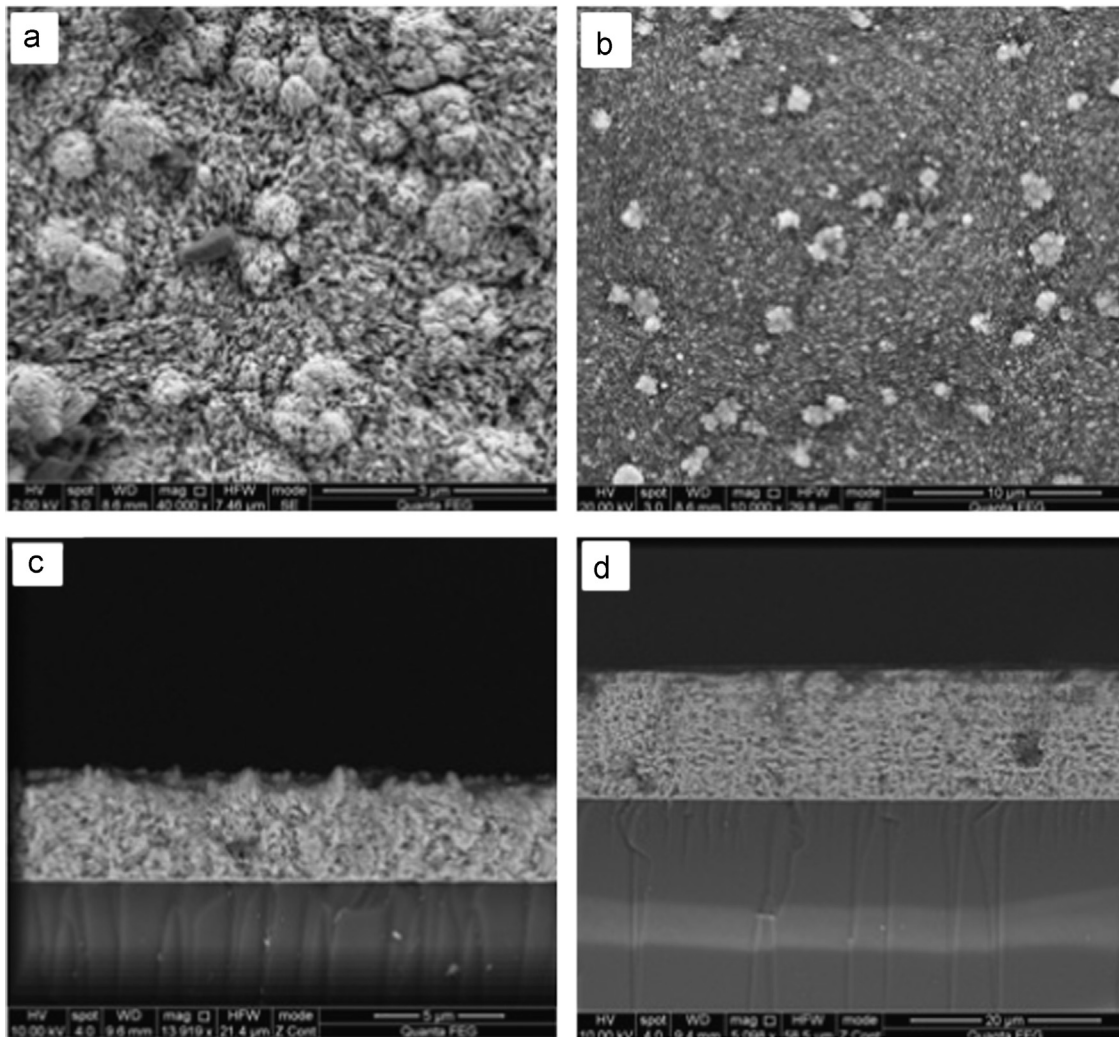| Sample	O %at.	Zn %at.	Ratio O/Zn
With air contact	56.07	43.93	1.28
Without air contact	50.37	49.63	1.01

Fig. 3. SEM micrographs of electrodes from: (a) sample 4 - top view; (b) sample 5 - top view; (c) sample 4 - cross sectional view; and (d) sample 5 - cross sectional view.
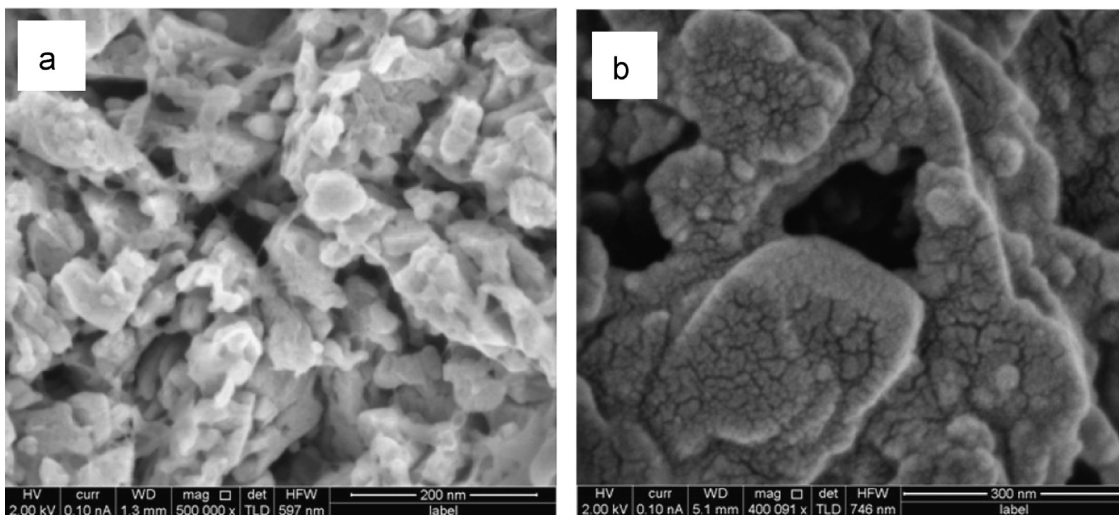

Fig. 4. High resolution SEM micrographs of an electrode from sample 5: (a) top view and (b) cross sectional.
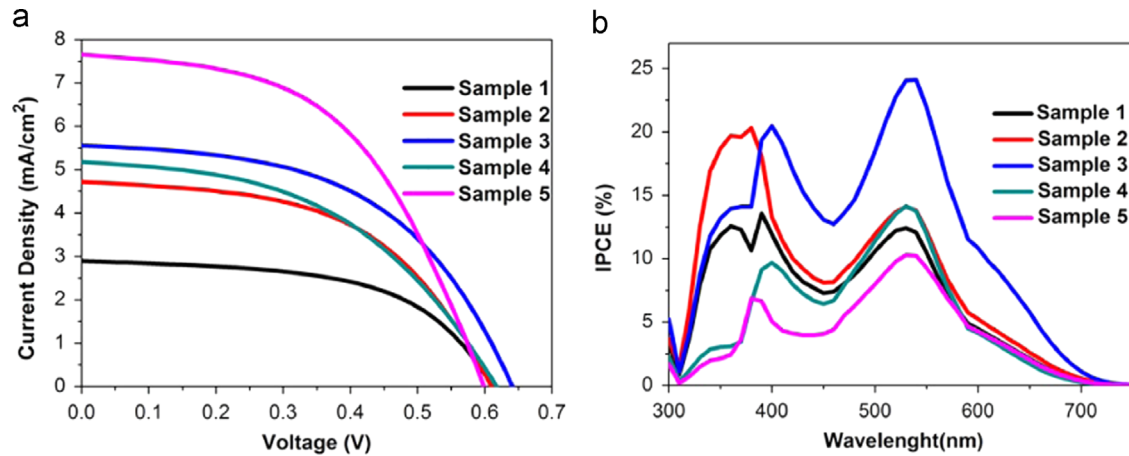
a

b

Fig. 5. (a) $J \times V$ curve and (b) IPCE spectra for the five samples.

Table 3
Photovoltaic parameters.

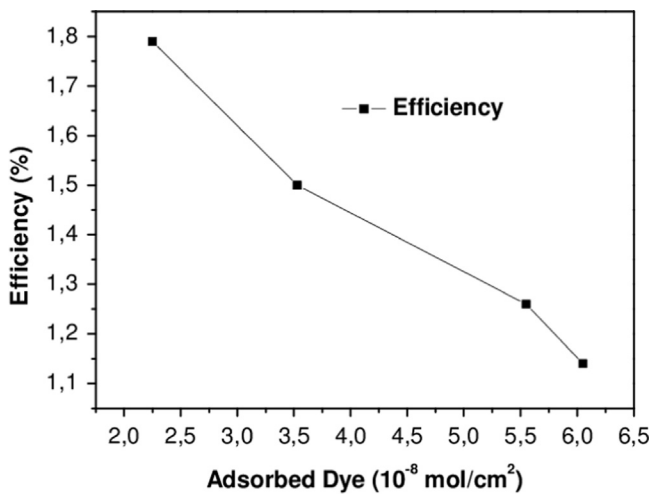| Sample	J_{SC} (mA/cm²)	V_{OC} (V)	FF (%)	PCE (%)	R_S (Ω cm²)	R_{Sh} (Ω cm²)
1	2.89	0.60	55.60	0.97	2.25	1.80
2	4.72	0.61	51.95	1.50	0.83	1.06
3	5.55	0.63	50.99	1.79	1.92	1.37
4	5.17	0.61	50.41	1.46	20.00	1.02
5	7.64	0.59	46.58	2.27	0.69	1.10

Fig. 6. Influence of dye adsorption on PCE values of solar cells.

lowest amount of dye adsorbed. This result can be explained by the dye precipitation on the ZnO nanostructure. According to Keis et al. [33] dye precipitation can take place on the ZnO nanostructure and, in this case, some dissolution of the ZnO by the acidic carboxylic groups of the dye can occur. The resulting Zn^{2+} ions form insoluble complexes with the N719 dye, causing precipitation of these complexes in the pores of the film. This gives rise to a filter effect (inactive dye molecules) [34].

4. Conclusions

ZnO thin films were synthesized by a low cost, electrodeposition technique, and used without any post-deposition treatment, to assembled DSCs. All the photoelectrodes were successfully used in DSCs. The morphological, structural and electrical characterization of the samples revealed the best performance for the more porous electrodes. The analysis of the amount of adsorbed dye reveals that a big amount of adsorbed dye decreases the PCE, probably due to the precipitation of the dye on the porous of the thin film. The devices present the feature to improve the PCE with the aging under ambient conditions. A remarkably high PCE 2.27% was obtained with the cell present with a mesoporous nanostructure. For this device the photovoltaic parameters were $V_{OC} = 0.59$ V, the $J_{SC} = 7.64$ mA/cm², FF = 50.41%, and the PCE = 2.27%.

References

[1] B. Cao, W. Cai, H. Zeng, G. Duan, Morphology evolution and photoluminescence properties of ZnO films electrochemically deposited on conductive glass substrates, J. Appl. Phys. 99 (2006) 073516.
[2] M. Zi, M. Zhu, L. Chen, H. Wei, X. Yang, B. Cao, ZnO photoanodes with different morphologies grown by electrochemical deposition and their dye-sensitized solar cell properties, Ceram. Int. 40 (2014) 7965–7970.
[3] C. Kung, H. Chen, C. Lin, Y. Lai, R. Vittal, K. Ho, Electrochemical synthesis of a double-layer film of ZnO nanosheets/nanoparticles and its application for dye-sensitized solar cells, Prog. Photovolt.: Res. Appl. 22 (2014) 440–451.

[4] X. Zou, Y. Liu, C. Wei, Z. Huang, X. Meng, Electrodeposition combination with hydrothermal preparation of ZnO films and their application in dye-sensitized solar cell, J. Chem. 820708 (2014).

[5] T. Yoshida, H. Minoura, Electrochemical self-assembly of dye-modified zinc oxide thin films, Adv. Mater. 12 (2000) 1219–1222.

[6] M.S. Akhtar, M.A. Khan, M.S. Jeon, O. Yang, Controlled synthesis of various ZnO nanostructured materials by capping agents-assisted hydro-thermal method for dye-sensitized solar cells, Electrochim. Acta 53 (2008) 7869–7874.

[7] I. Gonzalez-Valls, M. Lira-Cantu, Vertically-aligned nanostructures of ZnO for excitonic solar cells: a review, Energy Environ. Sci. 2 (2009) 19–34.

[8] M.H. Kumar, N. Yantara, S. Dharani, M. Graetzel, S. Mhaisalkar, P.P. Boiz, N. Mathewa, Flexible, low-temperature, solution processed ZnO-based perovskite solid state solar cells, Chem. Commun. 49 (2013) 11089–11091.

[9] B.N. Illy, A.C. Cruickshank, S. Schumann, R. Campo, T.S. Jones, S. Heutz, M.A. McLachlan, D.W. McComb, D.J. Riley, M.P. Ryan, Electrodeposition of ZnO layers for photovoltaic applications: controlling film thickness and orientation, J. Mater. Chem. 21 (2011) 12949–12957.

[10] T. Pauporté, C. Magne, Impedance spectroscopy study of N719-sensitized ZnO-based solar cells, Thin Solid Films 560 (2014) 20–26.

[11] I. Gonzalez-Valls, Y. Yu, B. Ballesteros, J. Oro, M. Lira-Cantu, Synthesis conditions, light intensity and temperature effect on the performance of ZnO nanorods-based dye sensitized solar cells, J. Power Sources 196 (2011) 6609–6621.

[12] S. Peulon, D. Lincot, Cathodic electrodeposition from aqueous solution of dense or open-structured zinc oxide films, Adv. Mater. 8 (1996) 166–170.

[13] S. Peulon, D. Lincot, Mechanistic study of cathodic electrodeposition of zinc oxide and zinc hydroxychloride films from oxygenated aqueous zinc chloride solutions, J. Electrochem. Soc. 145 (1998) 864–874.

[14] M.J. Zheng, L.D. Zhang, G.H. Li, W.Z. Shen, Fabrication and optical properties of large-scale uniform zinc oxide nanowire arrays by one-step electrochemical deposition technique, Chem. Phys. Lett. 363 (2002) 123–128.

[15] X. Qiu, L. Chen, H. Gong, M. Zhu, J. Han, M. Zi, X. Yang, C. Ji, B. Cao, The influence of annealing temperature on the interface and photovoltaic properties of CdS/CdSe quantum dot sensitized ZnO nanorods solar cells, J. Colloid Interface Sci. 430 (2014) 200–206.

[16] T. Pauporté, D. Lincot, Electrodeposition of semiconductors for optoe-lectronic devices: results on zinc oxide, Electrochim. Acta 45 (2000) 3345–3353.

[17] D. Lincot, Electrodeposition of semiconductors, Thin Solid Films 487 (2005) 40–48.

[18] J. Elias, R. Tena-Zaera, C. Lévy-Clément, Electrochemical deposition of ZnO nanowire arrays with tailored dimensions, J. Electroanal. Chem. 621 (2008) 171–177.

[19] H. Wei, H. Gong, Y. Wang, X. Hu, L. Chen, H. Xu, P. Liu, B. Cao., Three kinds of Cu_2/ZnO heterostructures solar cells fabricated with electrochemical deposition and their structure-related photovoltaic proper-ties, Crys. Eng. Commun. 13 (2011) 6065–6070.

[20] J. Elias, J. Michler, L. Philippe, M. Lin, C. Couteau, G. Lerondel, C. Lévy-Clément, ZnO nanowires, nanotubes, and complex hierarchical structures obtained by electrochemical deposition, J. Electron. Mater. 40 (2011) 728–732.

[21] M. Zhu, L. Chen, H. Gong, M. Zi, B. Cao, A novel TiO_2 nanorod/nanoparticle composite architecture to improve the performance of dye-sensitized solar cells, Ceram. Int. 40 (2014) 2337–2342.

[22] O. Lupan, V.M. Guérin, I.M. Tiginyanu, V.V. Ursaki, L. Chow, H. Heinrich, T. Pauporté, Well-aligned arrays of vertically oriented ZnO nanowires electrodeposited on ITO-coated glass and their integration in dye sensitized solar cells, J. Photochem. Photobiol. A 211 (2010) 65–73.

[23] J. Qiu, M. Guo, X. Wang, Electrodeposition of hierarchical ZnO nanorod–nanosheet structures and their application in dye-sensitized solar cells, ACS Appl. Mater. Interfaces 3 (2011) 2358–2367.

[24] V.M. Guérin, J. Rathousky, T. Pauporté, Electrochemical design of ZnO hierarchical structures for dye-sensitized solar cells, Sol. Energy Mater. Sol. Cells 102 (2012) 8–14.

[25] J. Xu, K. Fan, W. Shi, K. Li, T. Peng, Application of ZnO micro-flowers as scattering layer for ZnO-based dye-sensitized solar cells with enhanced conversion efficiency, Sol. Energy 101 (2014) 150–159.

[26] B. Xue, Y. Liang, L. Danglai, N. Eryong, S. Congli, F. Huanhuan, X. Jingjing, J. Yong, J. Zhifeng, S. Xiaosong, Electrodeposition from ZnO nano-rods to nano-sheets with only zinc nitrate electrolyte and its photoluminescence, Appl. Surf. Sci. 257 (2011) 10317–10321.

[27] Y. Lin, J. Yang, X. Zhou, Controlled synthesis of oriented ZnO nanorod arrays by seed-layer-free electrochemical deposition, Appl. Surf. Sci. 258 (2011) 1491–1494.

[28] W. Ludwig, W. Ohm, J. Correa-Hoyos, Y. Zhao, M. Lux-Steiner, S. Gledhill, Electrodeposition parameters for ZnO nanorods arrays for photovoltaic applications, Phys. Status Solid A 210 (2013) 1557–1563.

[29] M. Grätzel, Dye-sensitized solar cells, J. Photochem. Photobiol., C 4 (2003) 145–153.

[30] Y. Lin, J. Yang, Y. Meng, Nanostructured ZnO thin films by SDS-assisted electrodeposition for dye-sensitized solar cell applications, Ceram. Int. 39 (2013) 5049–5052.

[31] Y. Meng, Y. Lin, Y. Lin, Electrodeposition for the synthesis of ZnO nanorods modified by surface attachment with ZnO nanoparticles and their dye-sensitized solar cell applications, Ceram. Int. 40 (2014) 1693–1698.

[32] N.R. Neale, N. Kopidakis, J. Lagemaat, M. Grzätzel, A.J. Frank, Effect of a coadsorbent of the performance of dye-sensitized TiO_2 solar cells: shielding versus band-edge movement, J. Phys. Chem. B 109 (2005) 23183–23189.

[33] K. Keis, J. Lindgren, S.E. Lindquist, A. Hagfeldt, Studies of the adsorption process of Ru complexes in nanoporous ZnO electrodes, Langmuir 16 (2000) 4688–4694.

[34] A. Hagfeldt, G. Boschloo, L. Sun, L. Kloo, H. Pettersson, Dye-sensitized solar cells, Chem. Rev. 110 (2010) 6595–6663.